Geography and Sustainability 5 (2024) 329–342

Contents lists available at ScienceDirect

Geography and Sustainability

journal homepage: www.elsevier.com/locate/geosus

Research Article

Measuring urban thermal environment from accessibility-based perspective: A case study in a populous city

Xinyu Dong [a,b,c], Xiaoya Li [a], Yanmei Ye [a,*], Dan Su [a], Runjia Yang [a], Angela Lausch [b,c,d,e]

[a] Department of Land Management, Zhejiang University, Hangzhou 310058, China
[b] Department of Computational Landscape Ecology, Helmholtz Centre for Environmental Research–UFZ, Leipzig 04318, Germany
[c] Landscape Ecology Lab, Geography Department, Humboldt-Universität zu Berlin, Berlin 10099, Germany
[d] Department of Physical Geography and Geoecology, Martin Luther University Halle-Wittenberg, Halle 06120, Germany
[e] Department of Architecture, Facility Management and Geoinformation, Anhalt University of Applied Sciences, Dessau 06846, Germany

HIGHLIGHTS

- Spatial interaction effect among residents, UGS and HIA is considered.
- UGS has improved while HIA has shrunk within Zhengzhou's 3rd ring road.
- Notable mismatch between access to cooling service and heat exposure risk existed.
- Locations where residents are at extra heat exposure risk should be focused on.

GRAPHICAL ABSTRACT

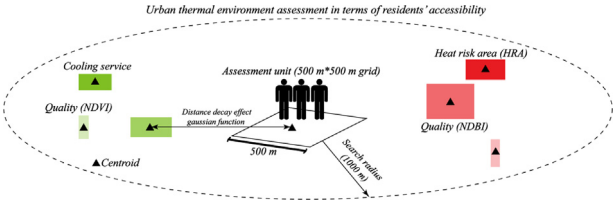

ARTICLE INFO

Article history:
Received 7 September 2023
Received in revised form 26 January 2024
Accepted 6 February 2024
Available online 20 February 2024

Keywords:
Urban heat island
Urban green space
Accessibility
Remote sensing
Spatial autocorrelation analysis

ABSTRACT

Understanding the spatial interaction among residents, cooling service, and heat risk area in complex urban areas is conducive to developing targeted management. However, traditional urban thermal environment assessments typically relied on simple linear integration of associated indicators, often neglecting the spatial interaction effect. To explore the spatial interaction among the three elements, this study proposes an accessibility-based urban thermal environment assessment framework. Using Zhengzhou, a rapidly urbanizing city, as an example, remotely sensed images from three periods (2010, 2015 and 2020) were applied to extract urban green space (UGS) and hot island area (HIA). An improved two-step floating catchment area (2SFCA) method and bivariate local Moran's *I* were employed to explore whether residents' clustering locations are more likely to access cooling service or to be exposed to heat risk. The results demonstrate that the UGS in the city has been expanding, whereas the HIA shrank within the inner city in 2015 and then increased in 2020. Even though the urban thermal environment may have improved in the last decade, the spatial interaction among the residents, cooling service and heat risk area could be exacerbated. Spatial autocorrelation shows an increase in locations that are disadvantageous for resident congregation. Even when sufficient cooling services were provided, residents in these areas could still be exposed to high heat risk. The developed urban thermal environment framework provides a novel insight into the residents' heat risk exposure and cooling service accessibility, and the findings could assist urban planners in targeting the improvement of extra heat exposure risk locations.

1. Introduction

Urbanization, one of the most direct reflections by economic growth and production development, has become a prominent issue worldwide (Zhang et al., 2019). United Nations data shows that in 2018, over half of the world's population resided in cities, a figure projected to rise to 68% by 2050 (DESA, 2018). The rapid expansion of cities, however, has given rise to a range of socioecological problems (Foley et al., 2005; Newbold et al., 2015). One of the most pressing among these is urban heat island (UHI) effect (Rajagopal et al., 2023; Zhang et al., 2021), the phenomenon by which city centers tend to be warmer than their rural surroundings (Martilli et al., 2020).

The increasing temperature could pose a profound threat to human health (Wong et al., 2017). Studies have consistently linked climate fluctuations to a variety of diseases, especially heat-related illnesses like

* Corresponding author.
E-mail address: yeyanmei@zju.edu.cn (Y. Ye).

https://doi.org/10.1016/j.geosus.2024.02.004

dehydration, heat exhaustion, and heatstroke. Such illnesses disproportionately affect vulnerable populations, including children, the elderly, and those with pre-existing medical conditions (Patz et al., 2005), leading to excess mortality (Conti et al., 2005; Tan et al., 2010). Such analogous increases in mortality due to heat exposure have been reported globally (Lee et al., 2018; Scortichini et al., 2018). This issue could be further exacerbated by the confluence of rapid urbanization and climate change, amplifying the threats faced by city residents (Liu et al., 2022; Nimac et al., 2022; Park et al., 2021a). Urban green space (UGS) is efficient in response to UHI effect, compared to other interventions such as cooling pavement materials and changes to urban morphology (Battista et al., 2023). Numerous studies and practices proved that UGS can significantly adjust the urban microclimate during hot summer periods. For instance, Smith et al. (2023) suggested that an increase in tree cover of 1% can create an average cooling effect of −0.089 K, and a 0.01 increase in albedo can contribute to an average cooling effect of −0.187 K. Similarly, Xi et al. (2023) found that a tree-grass ratio of 90% could reduce air temperature by up to 6 °C. Quality and quantity characteristics of UGS, such as vegetation greenness, landscape characteristics and proximity to green space also could substantially influence the cooling effect (Das et al., 2022; Liao et al., 2023).

Given its pivotal role in UHI alleviation, ensuring that all residents have adequate access to cooling services offered by UGS has become a growing concern. This issue has garnered the attention of scholars, urban planners, and policymakers, leading to the development of several quantification methods and frameworks (Yao et al., 2014). The two-step floating catchment area (2SFCA) method, commonly used to assess the accessibility of urban services such as parks, schools, and hospitals, is mainly based on a spatial supply-demand balance perspective, which could effectively identify geographical locations with potential disparities in resources. Hence, it has also been refined and employed to assess the rationality of spatial distribution of UGS (Xing et al., 2020; Zhang et al., 2022). For example, Yang et al. (2023) used the 2SFCA method to examine the street-level discrepancies in the supply and demand for UGS in Beijing, identifying key intervention areas where these imbalances were particularly pronounced.

Moreover, since the 2SFCA method can be combined with distance functions, including the Gaussian function and the Kernel function, researchers also have applied the improved 2SFCA method to spatially measure the residents' access to cooling service (Lan et al., 2022), which will attenuate with the proximity to UGS (Das et al., 2022; Liao et al., 2023; Yao et al., 2022). Despite the development of the accessibility-based cooling service assessment framework, quantification methods for residents' exposure to heat risk are mostly dependent on the simple summation or multiplication of associated indicators layers with varying weights, including socioeconomic data and UHI intensity (Chen et al., 2021; Tieskens et al., 2022; Shen et al., 2022; Li et al., 2022a; Zhu and Yuan, 2023). Residents, however, who cluster around, not within, the hot areas might also suffer from extra heat risk (Feng et al., 2019; Zhou et al., 2015). The spatial interaction between residents and warmer areas tends to be neglected in these heat risk evaluations involving linear integration.

In addition, UGS could significantly reduce surrounding temperature, as enumerated above, making it indeed negatively related between cooling services and heat exposure risk. Since the latter could also be regarded as cooling demand in terms of equity perspective, there is a propensity highlighting that neither should be isolated when measuring urban thermal environment in order to better target the mismatch area by the adaptive mitigation measure (Li et al., 2022a; Shen et al., 2022). Albeit this, numerous studies have tended to assess urban thermal environment from a single perspective with a coarse resolution, focusing either on cooling service supply or heat risk (B. Chen et al., 2022; Li et al., 2023; Park et al., 2021b). These studies with the coarse resolution failed to fully capture the comprehensive situation, and it therefore becomes challenging for urban planners to identify weak locations at the city level.

Consequently, based on the existing research gaps, the study aims to fully capture the urban thermal environment from two negatively related aspects, that is cooling service supply and heat risk exposure. In addition, the spatial interaction among residents, cooling service, and hot areas is incorporated, and by considering the spatial interaction effect, the primary objective of the study is to determine whether the spatial clustering pattern of residents is more advantageous in obtaining cooling services or more susceptible to heat risk exposure.

To achieve these objectives, we first retrieved UGS and land surface temperature (LST) using remotely sensed images. The hot island area (HIA) was further extracted from the retrieved LST by spatial autocorrelation analysis. An improved 2SFCA method was proposed to measure the accessibility-based cooling service supply and heat exposure risk. Lastly, we used bivariate local Moran's *I* to identify the locations where residents tend to garner more cooling service supply or suffer from extra heat exposure. A case study was designed in Zhengzhou China, a densely populated metropolis that is rapidly urbanizing, to demonstrate the effectiveness of the accessibility-based urban thermal environment assessment framework. Furthermore, to analyze the spatiotemporal trend of UGS, HIA, and residents' access to them, data from three periods (2010, 2015, 2020) was employed.

2. Materials and methods

2.1. Study area

Zhengzhou is a national central city, situated in central China. It is located at the demarcation point between the middle and lower reaches of the Yellow River, spanning 7,567 km^2. The city has a warm temperate continental monsoon climate, characterized by distinct seasons and an average annual rainfall of 632.8 mm. During high summer, the air temperatures could exceed 40 °C, making it prone to urban heat-related issues. As the political, economic and cultural center of Henan Province, Zhengzhou has grown dramatically in recent years, with an urbanization rate of nearly 80% and a population of over 12 million by the end of 2021. Rapid population growth and urban expansion, however, have resulted in a series of socioecological challenges. As a response, authorities formulated Zhengzhou Forest City Construction Master Plan (2011–2020), and the implementation has significantly increased in green areas across the city. Hence, Zhengzhou has been known as the green city. The study focuses on the five highly urbanized districts (see Fig. 1), covering an area of 1,080 km^2. In most Chinese cities, the ring roads represent the urban-suburban gradient, where the urbanization level and development intensity dwindle along the spatial gradient. According to the Worldpop data and nighttime light data in 2020, both the population density and the nighttime light brightness decrease along the urban-suburban gradient. In order to better understand the difference of thermal environment across different development levels, the study area was divided into four sub-groups based on the ring roads.

2.2. Methodology

The main focus of this study is on the spatial interaction effect of urban residents, UGS and HIA using accessibility-based assessment method, with the aim of exploring whether the spatial aggregation pattern of residents is more inclined to access cooling service or more exposed to heat risk.

Fig. 2 presents the methodological framework of the study, which is composed of three main components. The initial part involves the extraction of UGS and LST from Landsat data from three periods (2010, 2015, and 2020) which allows for an analysis of the spatiotemporal variation of the thermal environment. Getis-Ord Gi* spatial analysis is used to further distinguish the HIA based on the retrieved LST. The second component applies the improved 2SFCA method to spatially quantify residents' cooling service supply and heat exposure risk from accessibility-based perspective, aiming to capture the spatial interaction

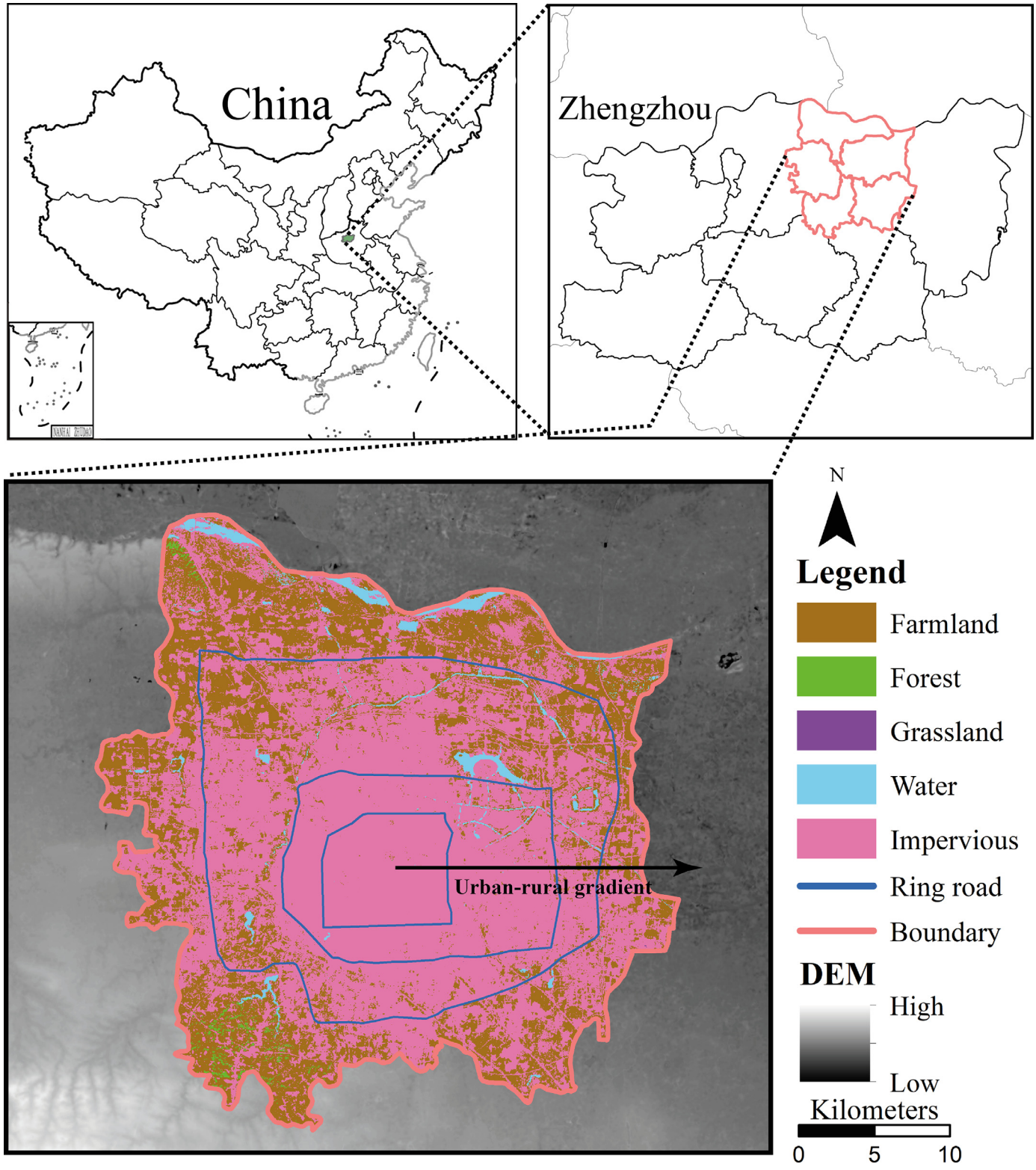

Fig. 1. Geographical location and boundary of study area.

effect between residents and the two elements. This method integrates the Gaussian function, normalized difference vegetation index (NDVI) and normal difference built-up index (NDBI) to indicate the distance decay effect, quality of cooling service and HIA, respectively. The population data, used in the method as the demand point, is from WorldPop while the supply point is determined by the extracted UGS and HIA in the last part. The objective of the third part is to identify and map the normal and abnormal spatial clustering pattern between cooling service supply and heat exposure risk by bivariate local Moran's *I*. The primary components exhibited in the Fig. 2 will be expatiated upon in

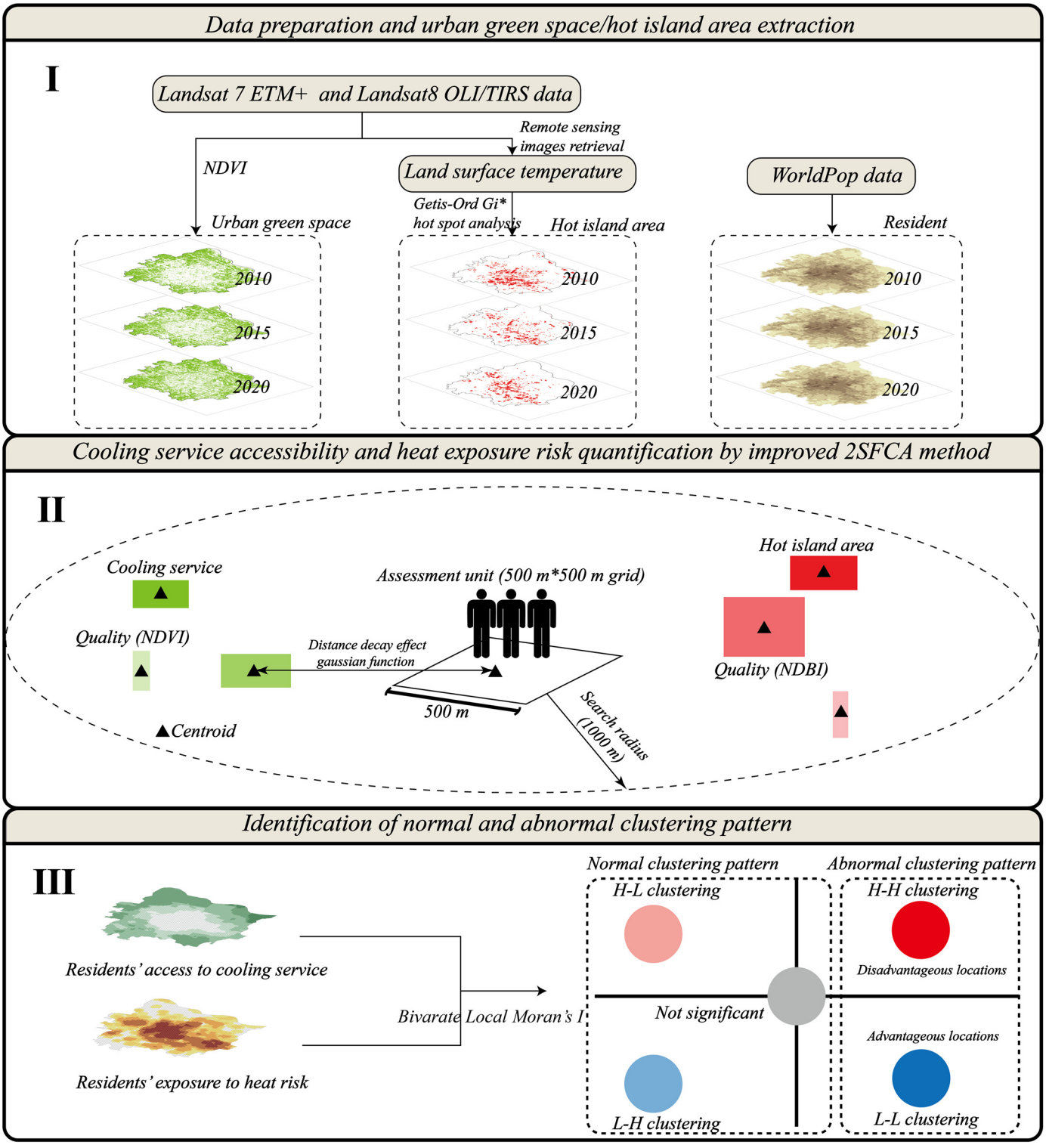

Fig. 2. Methodological framework of the study.

the following sections. Considering the data consistency and accuracy acceptability, the study sets grids with a resolution of 500 m as the basic assessment unit.

2.3. Data source and prepossessing

The population distribution data for the three periods was obtained from WorldPop with a resolution of 100 m, and according to the data statistics, the population within the study area was 4.03 million, 4.54 million and 5.07 million in 2010, 2015 and 2020, respectively. To maintain accuracy while minimizing complexity, we converted the resolution to 500 m, used each population grid as the basic assessment unit for the accessibility assessment. Zhengzhou experiences its comparatively hot period from April to October, characterized by a mean monthly air temperature exceeding 20 °C. As our study aims to analyze the most severe heat exposure risk, we downloaded imageries for these months during

the years 2010, 2015, and 2020, from the Landsat collection on the Google Earth Engine (GEE) platform. We then conducted a quality check for these remote sensing imageries using the quality assessment band and the mask of study area, and extracted imageries with a cloud cover within the study area of less than 5%. These remaining imageries were corrected using the FLAASH atmospheric correction module in ENVI software to minimize atmospheric noise. We also applied striping correction to the Landsat 7 ETM+ data. Finally, the ring roads for grouping the study area along the urban-rural gradient were retrieved from Open Street Map data.

2.4. Extraction of HIA and UGS

2.4.1. LST retrieval

The LST was retrieved using Landsat data by Radiative Transfer Equation (RTE) method. In comparison to other methods such as Single-channel method and Split-window method, the RTE approach has the advantage of accurately handling atmospheric path and atmospheric absorption effects, thereby enhancing its overall accuracy (Yu et al., 2014). After retrieving LST of all imageries, we composited the maximum values of the LST time series in order to reduce the uncertainty from a single imagery and reflect the most severe thermal situation across the whole year. The LST retrieval using RTE method can be expressed by Eq. (1) and Eq. (2) (Sekertekin, 2019):

$$B(T_s) = \frac{L_\lambda - L_\uparrow - \tau(1-\varepsilon)L_\downarrow}{\tau\varepsilon} \tag{1}$$

where L_λ is the at-sensor thermal infrared radiance; ε is the land surface emissivity; $B(T_s)$ is the emitted radiance for a black body at temperature T_s; $L_\uparrow$ is the upwelling radiance emitted by the surface and reflected by the atmosphere; $L_\downarrow$ is the downwelling radiance received by the sensor; τ is atmospheric transmission. The atmospheric parameters τ, $L_\uparrow$ and $L_\downarrow$ could be obtained from an online atmospheric correction tool, Atmospheric Correction Parameter Calculator, developed by NASA (https://atmcorr.gsfc.nasa.gov/). The calculator can output the atmospheric transmission, upwelling and downwelling radiance based on location and time information.

Further, T_s can be finally calculated from $B(T_s)$ by plank's law:

$$T_s = \frac{K_2}{\ln\left(K_1/B(T_s)+1\right)} \tag{2}$$

where T_s is the land surface temperature in Kelvin; K_1 and K_2 are constants.

2.4.2. UGS and HIA identification

The urban-rural dichotomy method has been widely used in UHI effect identification. This approach, however, has the weakness of subjectively defining rural and urban demarcations, making it challenging to be utilized in highly urbanized areas that lack a distinct rural context. Furthermore, Martilli et al. (2020) suggested that, instead of focusing on the temperature gap between rural and urban areas, which is a relative value, UHI effect mitigation studies should prioritize the specific heat indicators. For these reasons, we applied Getis-Ord Gi* spatial analysis, an objective UHI identification method proposed by Zhang et al. (2015), to identify the HIA. We processed all retrieved LST data at a 100 m resolution for the spatial clustering analysis. Only the high-high (H-H) spatial clustering pattern was remained and further analyzed. Then, the contiguous H-H clustering grids were merged into a single unit and extracted as HIA. The Getis-Ord Gi* spatial analysis can be expressed by Eq. (3).

$$G = \frac{\sum_{i=1}^{n}\sum_{j=1}^{n} W_{ij}x_i x_j}{\sum_{i=1}^{n}\sum_{j=1}^{n} x_i x_j} \tag{3}$$

where G is the value of the local Getis-Ord Gi*, and the grids pass the z-test (z score is above 2.58) under p-value < 0.01 were extracted; $x_i$and x_j are the LST on the ith and jth grid respectively ($i \neq j$); w_{ij} is the spatial weight matrix; n is the sum of grids.

Non-park green space is an essential source of cooling service, often neglected in previous studies on cooling service (M. Chen et al., 2022; Yan et al., 2018; Yao et al., 2022). Nevertheless, these spaces play a crucial role in promoting spatial equity (Ke et al., 2023), a primary focus in this study. Thus, we concentrated on the cooling service provided by general UGS rather than green parks. NDVI is an efficacious indicator for vegetations extraction, and we designated areas with NDVI over 0.4 as UGS (Lan et al., 2022). NDVI can be calculated from Landsat imageries by Eq. (4):

$$\mathrm{NDVI} = (\mathrm{NIR} - \mathrm{RED})/(\mathrm{NIR} + \mathrm{RED}) \tag{4}$$

where NIR is the band 4 and band 5 for Landsat 7 and Landsat 8 images respectively; RED is the band 3 and band 4 for Landsat 7 and Landsat 8 images, respectively.

For the validation of the UGS identified in the three periods, three groups of 200 random samples of vegetation and non-vegetation were selected in Google Earth high resolution historical imageries. The kappa coefficients, which represent classification accuracy, of vegetation and non-vegetation were 0.82, 0.79 and 0.83 for 2010, 2015 and 2020, respectively, which are all above 0.6, demonstrating an acceptable level of goodness-of-fit (Chmura Kraemer et al., 2002).

2.5. Quantification of cooling service supply and heat exposure risk

2SFCA, first introduced by Radke and Mu (2000) and later formalized by Luo and Wang (2003), originally assesses accessibility to healthcare facility. Currently, it has wider applications in assessment of rationality of spatial resource distribution, such as flooding risk pressure and cooling service (Lan et al., 2022; Yang et al., 2023), etc.

The traditional 2SFCA method consists of two steps. In the first step, for a given search radius, the supply-to-demand ratio is calculated for each supply point. Specifically, for the ith supply point, the ratio of the supply point to the demand points within the search radius is calculated. This yields a supply-to-demand ratio for each supply point.

The second step sums these ratios to estimate the level of accessibility for each demand point. Specifically, for the jth demand point, the sum of all supply-to-demand ratios calculated in the first step, over all supply points within the search radius, is used as an estimate of the accessibility of the demand point. By aggregating the supply-to-demand ratios, the 2SFCA method can provide a comprehensive assessment of accessibility that considers the spatial distribution of both demand and supply points. In this study, UGS and HIA are considered as the supply point while population data are treated as the demand point.

The residents' access to cooling service is quantified based on three factors, including ratio of area to population and quality of UGS and distance. The most important element is the ratio of area of UGS to population within the search radius because the cooling capacity of UGS is limited at a given area, and a larger population indicates a higher anthropogenic heat emission, equal to a higher load for the cooling service. Moreover, studies have demonstrated that the cooling effect of UGS is strongly correlated with NDVI than other characteristics (Das et al., 2022; Xiao et al., 2023), making NDVI the most applicable to represent the cooling quality of a UGS. In addition, researches have found that the cooling effect will decrease with increasing distance from UGS, and the Gaussian function was therefore employed to generalize the decay effect as the distance increases (Yan et al., 2018). The study defined that the maximum decay distance for cooling effect is 1 km. The calculation for residents' access to cooling service is presented as Eq. (5):

$$A_i^{\mathrm{CS}} = \sum_{j=1}^{n} \frac{S_j^{\mathrm{UGS}} \cdot \left(1 + \overline{\mathrm{NDVI}_j}\right) \cdot f(d_{ij})}{\sum_{k=1}^{m} D_k \cdot f(d_{kj})} \tag{5}$$

where A_i^{CS} is the residents' access to cooling service on the ith grid; S_j^{UGS} is the area of the jth UGS; $\overline{NDVI_j}$ is the mean normalized difference vegetation index of the jth UGS representing the cooling quality; $f(d_{ij})$ is the Gaussian function, as shown by Eq. (6), reflecting the decay effect of cooling service along with the distance; $\sum_k^m D_k$ is the total population within the 1 km search radius of the jth UGS; the higher the value of A_i^{CS}, the more the surrounding cooling services available to the residents in the ith location.

$$f(d_{ij}) = \begin{cases} \frac{e^{-1/2\times(d_{ij}/d_0)^2} - e^{-1/2}}{1-e^{-1/2}}, d_{ij} \le d_0 \\ 0, d_{ij} > d_0 \end{cases} \quad (6)$$

Similar to the quantification of cooling service, we also quantified the accessibility-based heat exposure risk from three aspects, including area of HIA, quality and population within given distance. For the purpose of maintaining a same interval as NDVI, we applied NDBI, which is positively correlated with the LST, to indicate the quality of HIA (Dutta and Das, 2020; Halder et al., 2021). Heat exposure risk also could decay along with the proximity to heat sources, which is represented by the Gaussian function (Feng et al., 2019; Zhou et al., 2015), and in order to equally measure the spatial interaction effect among the three elements, we assigned the decay distance of HIA is consistent with the cooling service. The NDBI is calculated by Eq. (7), and the quantification of accessibility-based heat exposure risk is shown in Eq. (8):

$$NDBI = (SWIR - NIR)/(SWIR + NIR) \quad (7)$$

where SWIR is band 5 and band 6 for Landsat 7 and Landsat 8 images, respectively. NIR is same with that in Eq. (4).

$$A_i^{HIA} = \sum_{j=1}^{n} \left[S_j^{HIA} \cdot \left(1 + \overline{NDBI_j}\right) \cdot \sum_{k=1}^{m} D_k f(d_{kj}) \right]^{1/2} \cdot f(d_{ij}) \quad (8)$$

where A_i^{HIA} is the accessibility-based residents' heat exposure risk of on the ith grid; S_j^{HIA} is the area of the jth HIA; $\overline{NDBI_j}$ is the mean NDBI of the jth HIA representing the quality; $f(d_{ij})$ is the Gaussian function, as shown by Eq. (6), reflecting the decay effect of heat risk along with the distance; the higher the value of A_i^{HIA}, the higher the surrounding heat exposure risk to the residents in the ith location.

Note that unlike the quantification of residents' cooling service supply, the first step of heat exposure risk is calculated as a multiplication rather than a division, which means that for the jth HIA, the higher the population within search radius, the more hazardous the HIA. The higher the A_i^{HIA}, the higher the residents' heat exposure risk.

2.6. Spatial autocorrelation analysis

Local spatial autocorrelation analysis is an effectively measure to detect similarities and correlations between spatial units and their surroundings, distinguish spatial clustering and isolation, and examine spatial unevenness (Wang et al., 2021).

We used bivariate local Moran's I to investigate the spatial clustering pattern between residents' cooling service supply and heat exposure risk. The basic unit for the spatial autocorrelation analysis is 500 m^2 grids. The expression of bivariate local Moran's I is shown as Eq. (9):

$$I_{kl} = \frac{x_k^i - \overline{x}_k}{S_k^2} \times \sum_{i=1}^{n} \sum_{j=1}^{n} w_{ij} \times \frac{x_l^j - \overline{x}_l}{S_l^2} \quad (9)$$

where I_{kl} is the value of bivariate local Moran's I; x_k^i is the cooling service accessibility on the ith grid; x_l^j is the accessibility-based heat risk on the jth grid ($i \neq j$); $\overline{x}_k$ and $\overline{x}_l$ are the mean of cooling service and accessibility-based heat risk, respectively; w_{ij} is the spatial weight matrix; S_k^2 and S_l^2 are variance of residents' access to cooling service and accessibility-based heat exposure risk, respectively; n is the sum of grids.

The bivariate local spatial autocorrelation analysis results can be exhibited by the bivariate local indicators of spatial association (BiLISA) map, which comprises four clustering categories: high-high (H-H), high-low (H-L), low-high (L-H), and low-low (L-L). Generally, adequate UGS could significantly lower the surrounding temperature. Hence, residents who benefit from sufficient cooling service supply tend to suffer from less heat exposure risk, and vice versa. Therefore, the H-L, L-H and not significant are normal spatial patterns, whereas the H-H and L-L are the abnormal clustering patterns. The former implies a disadvantageous location and suggests that residents could experience higher heat exposure risk despite the sufficient cooling service supply while the later indicates an advantageous location where residents would face less heat exposure risk albeit relatively lower cooling service supply. Referring to (Li et al., 2022b), we used the z-score of Moran's I to further distinguish the abnormal clustering patterns: moderately extra heat risk exposure ($1.96 < z\text{-score} < 2.58$); strongly extra heat risk exposure ($z\text{-score} > 2.58$); moderately cooling service supply ($-2.58 < z\text{-score} < -1.96$); strongly extra cooling service supply ($z\text{-score} < -2.58$).

3. Results

3.1. Identification of UGS and HIA

3.1.1. Spatiotemporal variation in UGS

The spatiotemporal variations in UGS are depicted in Fig. 3(a–c). There is a significant spatial unevenness of UGS along the urban-rural gradient. On the whole, UGS coverage increased from the inside to the outside, and the trend remained unchanged for the three periods. In 2010, UGS was deficient and sparsely distributed within the core areas. Particularly inside the 2nd and 3rd ring roads, the coverage was merely 11.4% and 18.0%, respectively. UGS, however, has experienced a drastic increase in the last decade, especially within the 3rd ring road. For instance, the coverage nearly tripled to 29.1% inside the 2nd ring road and almost doubled to 34.6% between the 2nd to 3rd ring road in 2020, compared to the coverage in the first period. Albeit the most striking enhancement, the UGS was still insufficient within 3rd ring road compared to the peripheral areas. Beyond the 4th ring road, the improvement in UGS was comparatively modest, only rising by 6.4%, from 61.9% to 68.3% over the past decade. This was a less pronounced trend compared to that within the 3rd ring road. Generally, the improvement of UGS was more significant within the core areas, and the gap between the inner and the marginal areas has shrunk.

3.1.2. Spatiotemporal variation in HIA

The spatiotemporal trend of HIA is shown in Fig. 3(d–f). Similar to UGS, HIA also exhibits a significant spatial heterogeneity along the urban-rural gradient. HIA was mostly concentrated within the inner city, and its coverage decreased from the inside to the outside, showing a trend inverse to that of UGS. Generally, the temporal changes were significant. The highest HIA coverage was found in 2010, accounting for 35.3%, 28.5%, 9.4%, and 4.5% in the four spatial gradient zonings, respectively. In contrast, HIA was more sporadically scattered in 2015, especially in the central areas where the coverage was 26.6% and 15.6% inside the 2nd ring road and between the 2nd ring road to the 3rd ring road, respectively, significantly lower than in the other two periods. HIA changes over the three periods were not as consistent as those of UGS in some respects. For instance, the trend of HIA within the 3rd ring road was not monotonic. It first decreased in 2015 and then increased in 2020. In addition, the spatial pattern differed from each period. In 2010, HIA was mostly concentrated in the south-central part of the city with some distributed in the north (Fig. 3(d)). However, by 2020, HIA was most concentrated inside the 2nd ring road, and there was almost no HIA observed beyond the 4th ring road (Fig. 3(f)). However, from spatial gradient perspective, the pronounced changes of HIA occurred inside the 3rd ring road, while the variations in peripheral areas were not significant, which was similar to those of UGS.

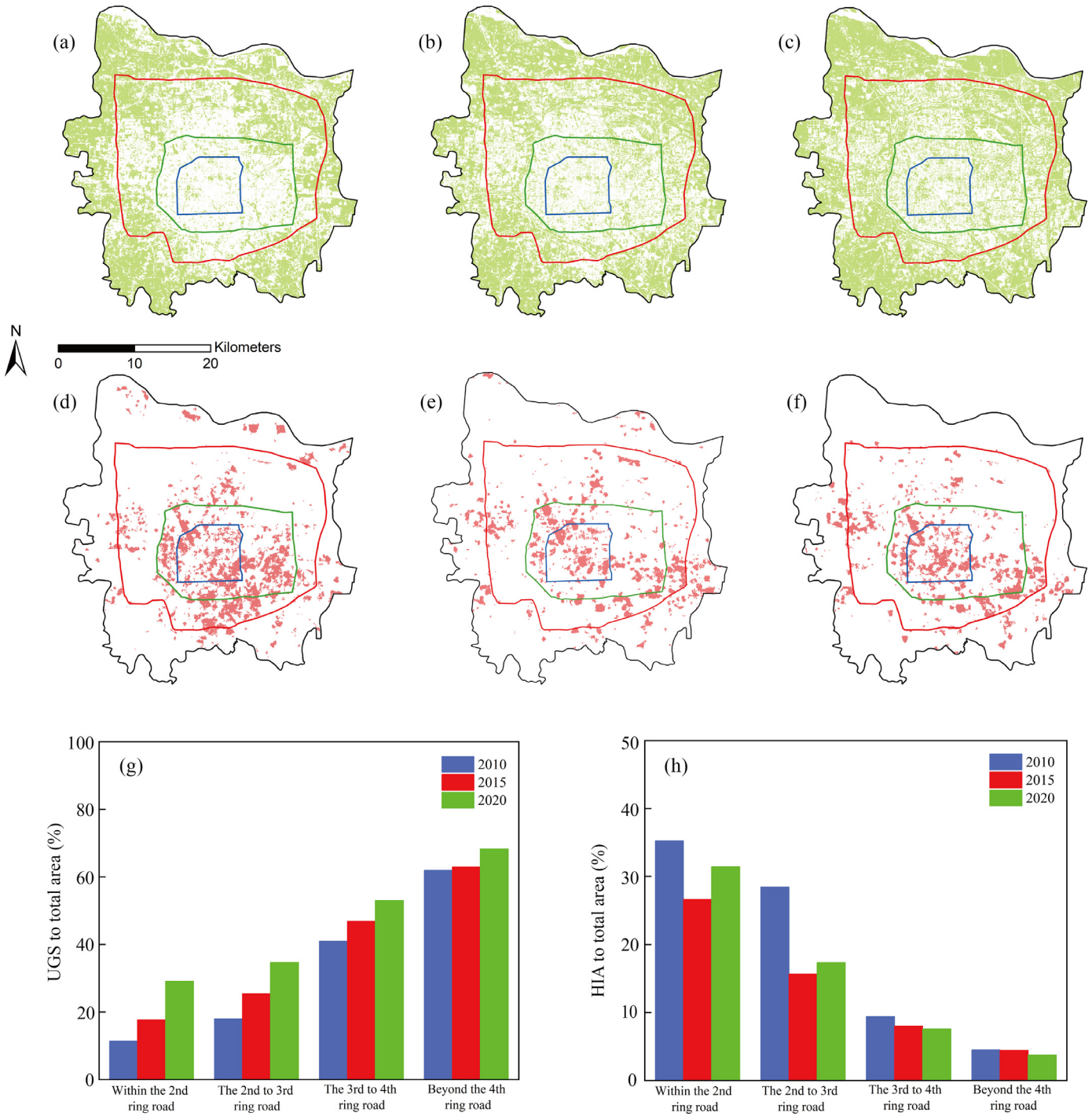

Fig. 3. Spatiotemporal variation in UGS and HIA. (a)–(c) spatiotemporal variation in UGS in 2010, 2015 and 2020, respectively; (d)–(f) spatiotemporal variation in HIA in 2010, 2015 and 2020, respectively; (g) and (h) variation in ratio of UGS and HIA to total area, respectively. The colored lines in (a)–(f) are consistent with these in Fig. 2.

3.2. Accessibility-based thermal environment assessment

3.2.1. Spatiotemporal variation in cooling service accessibility

Fig. 4 (a–c) illustrates the spatial pattern of accessibility-based cooling service for the three periods. Each grid in Fig. 4 corresponds to a specific statistic, further demonstrated in Fig. 5 through log-transforming. The wider sections of these violin plots represent a higher probability. Moreover, the descriptive statistics of these grids is shown in Table 1. The range of statistics unit of the table, including zone I, II, III and IV, is indicated in Fig. 4. We applied coefficient of variation (C.V) to indicate the evenness of the cooling service accessibility. The higher the C.V, the more unequal the available cooling service to residents.

The cooling service accessibility shows a similar spatial pattern over the three periods, gradually increasing from the inner out. The spots with lower cooling service accessibility were mostly located in the inner city. Nearly all locations had the lowest cooling service accessibil-

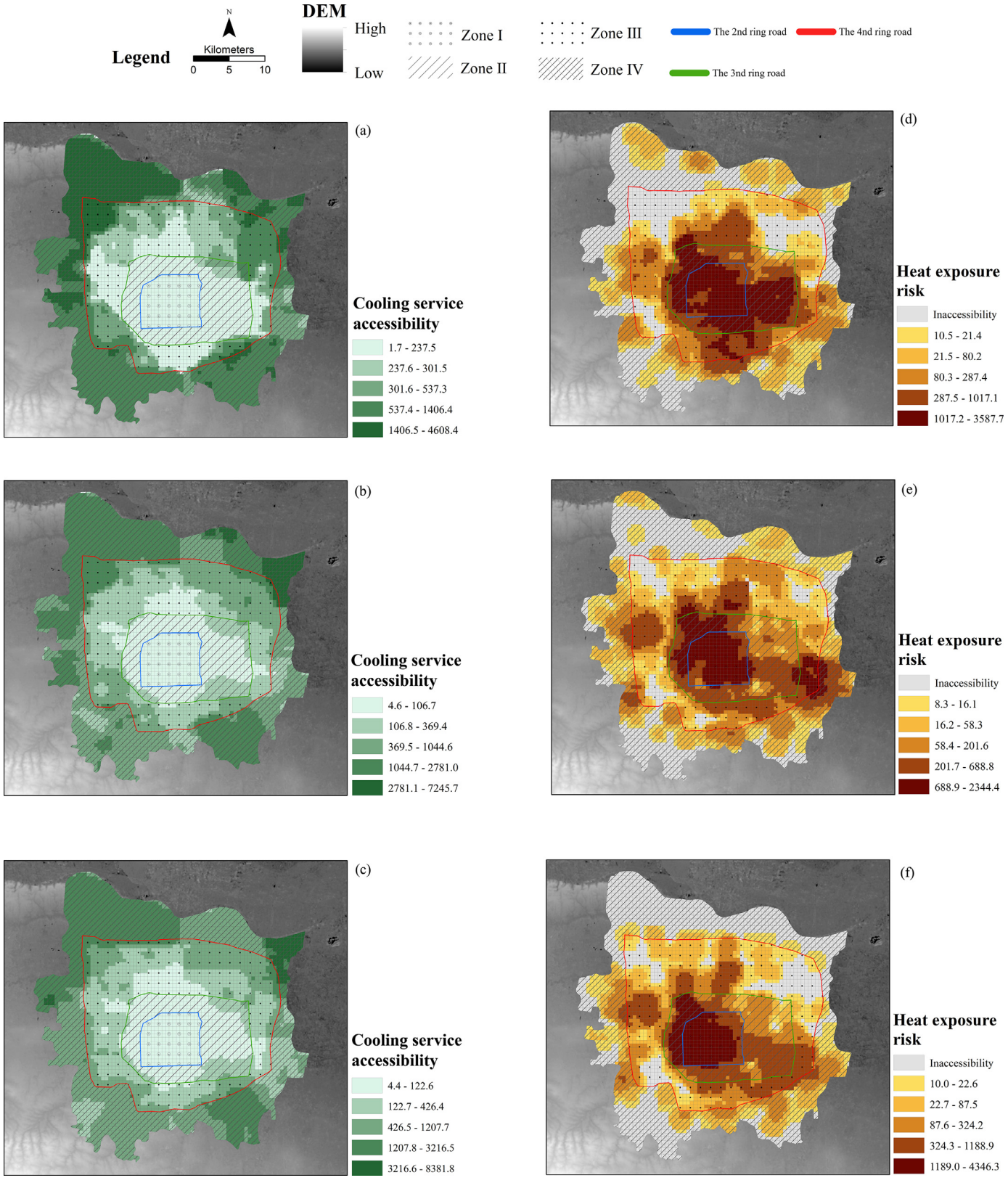

Fig. 4. Residents' access to cooling service (a)–(c) and heat exposure risk (d)–(f); the colored lines are consistent with these in Fig. 2.

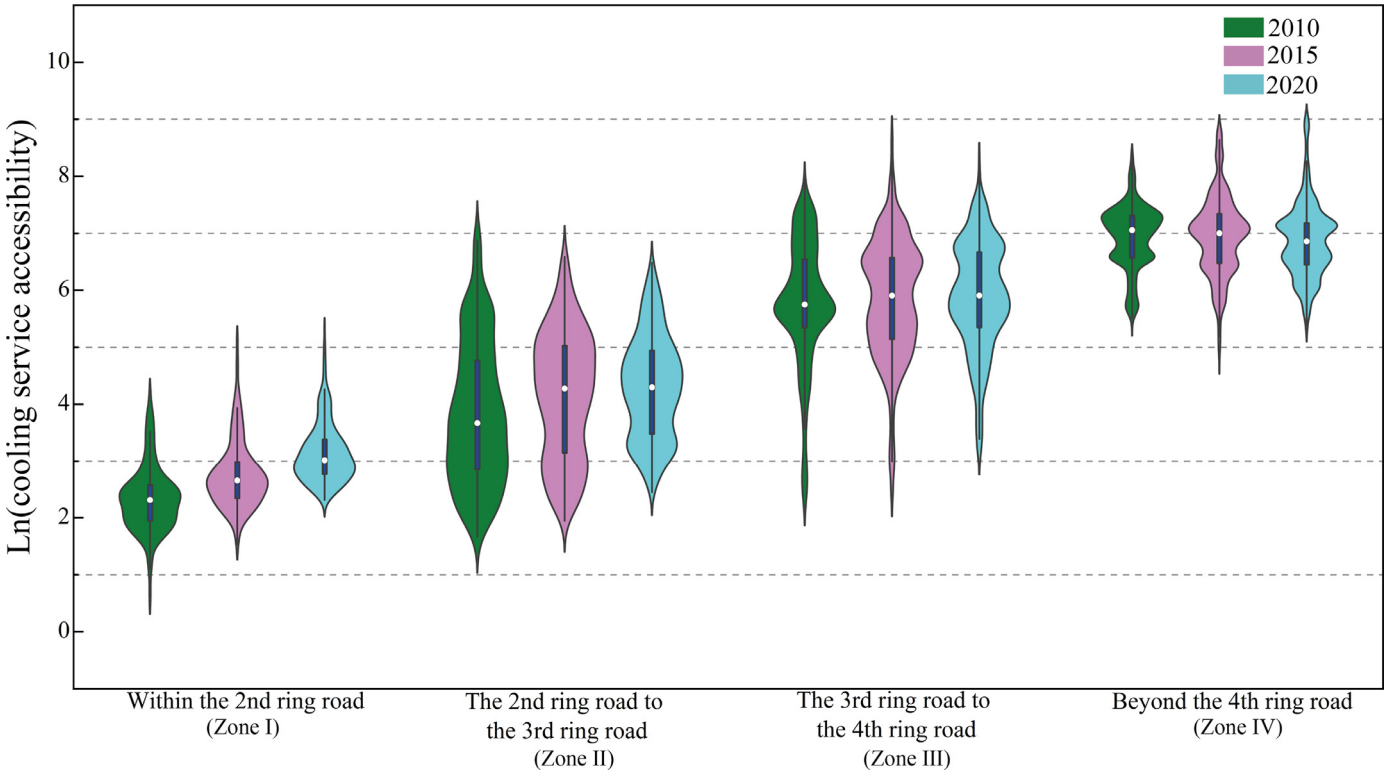

Fig. 5. Violin plots of residents' cooling service accessibility; the white points and the boxes within each violin plot show the median values and the 95% confidence intervals; the width of each violin plot at any given point represents the density of data points at that value.

Table 1
Descriptive statistics of cooling service accessibility.

Year	Zone	Max	Min	Median	Average	C.V
2010	Zone I	67.5	1.7	10.8	12.4	0.63
	Zone II	966.0	5.2	39.2	103.4	1.08
	Zone III	2,958.5	7.9	314.0	513.9	0.85
	ZoneIV	4,608.4	43.0	1,158.9	1,185.4	0.43
2015	Zone I	175.8	4.6	14.2	19.3	0.80
	Zone II	723.2	6.9	72.0	110.5	0.96
	Zone III	6,521.5	9.3	367.5	555.2	0.94
	ZoneIV	7,245.7	37.5	1,097.1	1,337.4	0.65
2020	Zone I	213.2	4.4	20.4	27.2	0.65
	Zone II	655.1	11.5	73.5	109.1	0.90
	Zone III	4,618.1	20.3	368.1	540.8	0.82
	Zone IV	8,381.8	52.0	958.5	1,245.2	0.69

Abbreviation: coefficient of variation (C.V).

ity level. In contrast, the highest cooling service accessibility level in the three periods were all observed in zone IV, which were 4,608.4, 7,245.7, and 8,381.8 in 2010, 2015 and 2020, respectively. Within zone I, the maximum available cooling service rose from 67.5 to 213.2 in the last decade, and the highest probability density of the accessibility also substantially increased (Fig. 5), demonstrating that the residents' access to cooling service has significantly improved in the urban central areas. Albeit the pronounced improvement, the gap along the urban-rural gradient was still significant. For example, average accessibility levels within zone I were 12.4, 19.3 and 27.2, respectively. Comparatively, the average accessibility levels within zone IV were 1,185.4, 1,337.4 and 1,245.2, respectively. Notably, the median of cooling service in zone IV in turn declined over the period. In addition, the probability distribution shows multiple peaks in the zone, implying that residents may have significantly unequal access to cooling services.

The C.V decreased in zone I, II and III, demonstrating that the inequality of cooling service accessibility gradually tapered off, whereas the changes of C.V exhibited an opposite trend in zone IV, increasing from 0.43 in 2010 to 0.69 in 2020.

3.2.2. *Spatiotemporal variation in accessibility-based heat exposure risk*

Fig. 4 (d–f) illustrate the spatial patterns of residents' heat exposure risk across the three periods, with corresponding descriptive statistics shown in Table 2. A similar spatial pattern in the three periods was observed. The heat exposure risk gradually fell from the inner to the outer areas. The heat exposure risk was most severe in zone I, and almost all locations in the zone displayed the highest heat exposure risk level. All residents within the 2nd ring road were exposed to heat risk even in 2015 when the HIA coverage and average accessibility level (1,139.1) were most moderate. Nevertheless, beyond the 4th ring road, more than half the areas (51.7%) no longer suffered from heat exposure risk in 2020. Although the HIA coverage inside the 2nd ring road was less in 2020 than in 2010, the average heat exposure risk levels were higher in 2020 than in 2010, reaching 2,013.5. The peak of probability density

Table 2
Descriptive statistics of heat exposure risk.

Year	Zone	Max	Min	Median	Average	C.V	Proportion of non-exposure area (%)
2010	Zone I	3,587.7	353.8	1,703.9	1,769.3	0.42	0
	Zone II	3,378.2	37.3	1,044.7	1,221.4	0.62	1.5
	Zone III	2,328.1	20.0	211.7	366.1	0.89	23.8
	Zone IV	1,104.6	10.8	52.0	95.8	1.10	41.1
2015	Zone I	2,267.9	184.5	1,123.2	1,139.1	0.47	0
	Zone II	2,344.4	38.7	344.7	474.8	0.79	0
	Zone III	1,102.3	16.2	119.0	215.4	0.93	11.0
	ZoneIV	969.7	8.3	44.4	104.0	1.17	35.6
2020	Zone I	4,346.3	189.5	2,185.4	2,013.5	0.47	0
	Zone II	3,150.1	39.5	485.5	683.1	0.82	1.2
	Zone III	1,664.7	20.3	152.3	235.6	0.88	17.1
	Zone IV	730.7	10.0	55.6	111.5	0.98	51.7

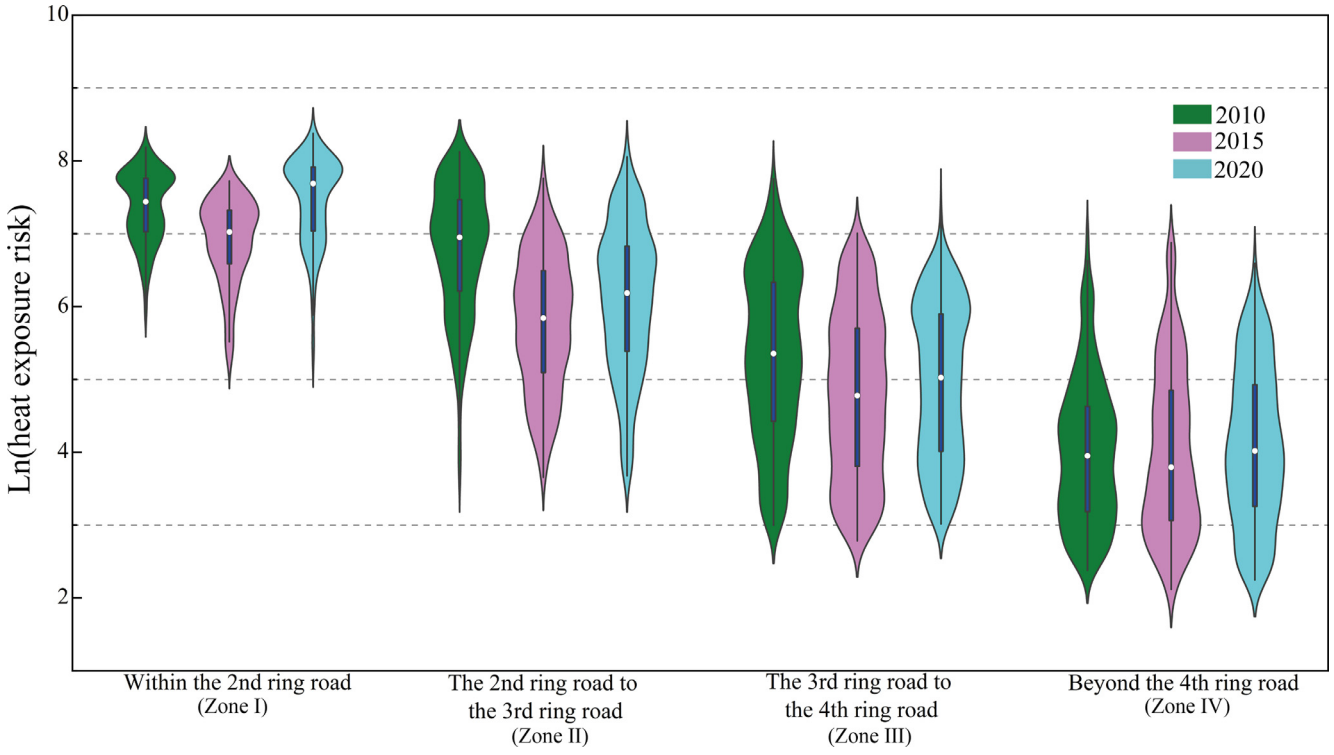

Fig. 6. Violin plots of residents' heat exposure risk; the white points and the boxes within each violin plot show the median values and the 95% confidence intervals; the width of each violin plot at any given point represents the density of data points at that value.

was also significantly higher in 2020, suggesting a growing number of residents in zone I were suffering from the higher heat exposure risk (as shown in Fig. 6(a)). Also, the maximum heat exposure risk in zone I was found in 2020, which was 4,346.3 compared to 3,587.7 and 2,267.9 in 2010 and in 2015, respectively. However, despite the improvement in cooling service accessibility, the residents' heat exposure risk in the inner city actually worsened.

The C.V of heat exposure risk was highest in zone IV. In fact, more residents in the periphery were no longer exposed to heat risk, suggesting that the inequality of heat exposure risk in the marginal areas was significantly greater than in the core areas.

3.3. Identification of abnormal clustering pattern

The BiLISA maps for the three periods are shown in Fig. 7 (a–c) and the statistics of the abnormal and normal clustering patterns are exhibited by Fig. 7(d) and (e), respectively. The spatial clustering patterns exhibit a significant spatial unevenness along with the urban-rural gradient. Nearly all locations within the 3rd ring road were L-H clustering, i.e. lower cooling service accessibility coupling with higher heat exposure risk. This indicated residents in the zone were still suffering from high heat exposure risk though the UGS has sharply increased from 2010 to 2020. Although the L-H clustering still extensively existed, the grids with no clustering pattern namely not significant, which could be considered as medium level for cooling service accessibility and heat exposure risk, were also prevailing in zone III (between the 3rd ring road to the 4th ring road), suggesting that the thermal comfort may have comparatively improved.

It should be noted that a significant spatial heterogeneity was observed between the 3rd and 4th ring roads where the four clustering categories and insignificant areas were all present in a certain proportion in the three periods. From the inner out, the normal clustering patterns gradually transformed from L-H to not significant to H-L, and the spatial trend was consistent over the three periods. Beyond the 4th ring road where the heat exposure risk was lower under plentiful cooling service supply, most spatial clustering patterns were H-L and insignificant

The abnormal clustering patterns, namely H-H and L-L clustering were mainly aggregated around the 4th ring road, especially the H-H

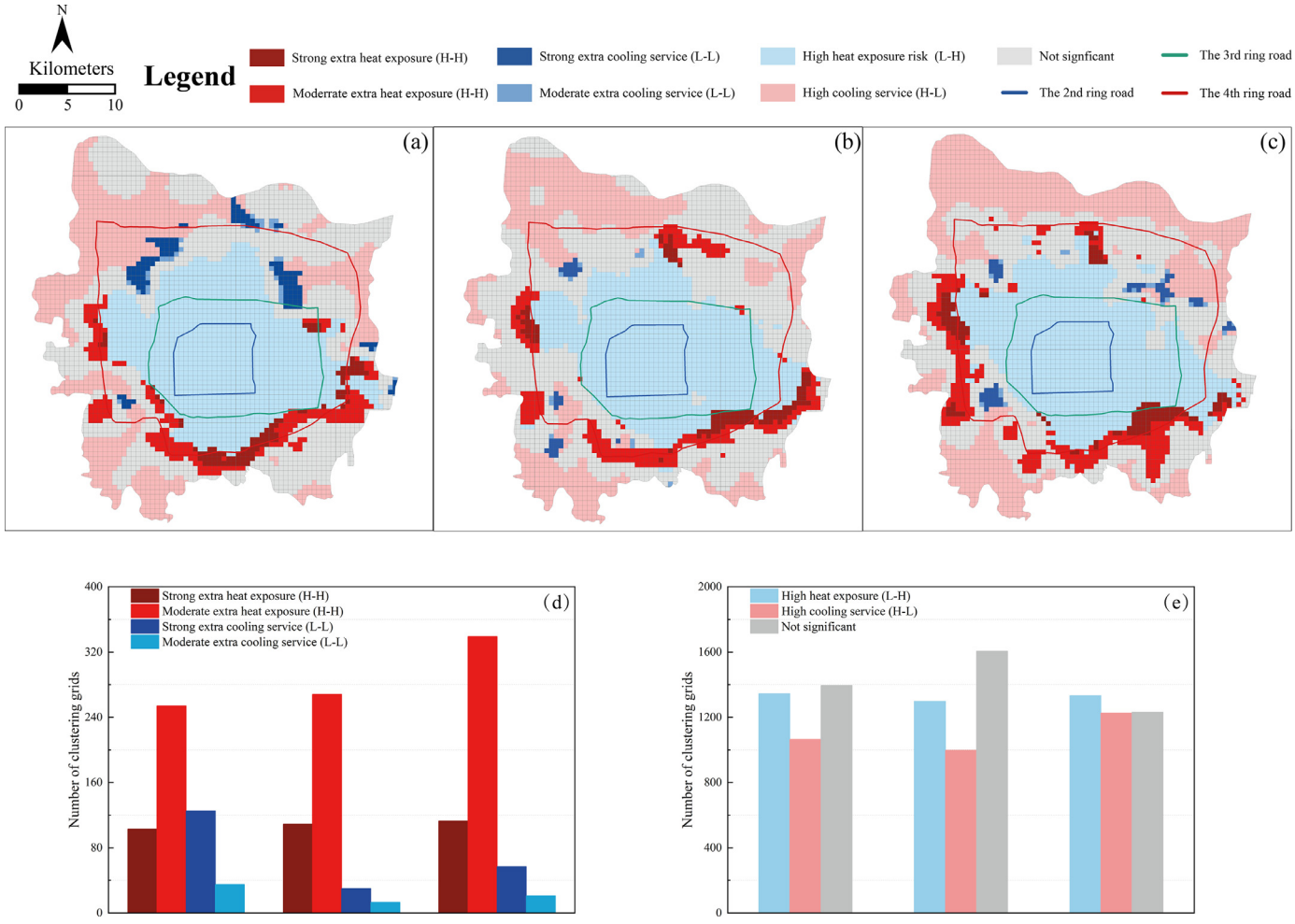

Fig. 7. BiLISA map for the three periods. (a) 2010; (b) 2015; (c) 2020; (d) and (e) sum of the normal and abnormal clustering, respectively.

clustering in the three periods. The total number of the H-H clustering was 357, 377 and 452 in 2010, 2015 and 2020, respectively, among which moderate extra heat exposure risk spots were minor, while the strong extra heat exposure risk spots were preponderant, but both exhibited a monotonical increase trend. Almost all L-L clustering was primarily gathered within the zone III, and slumped in 2015 and 2020 compared to the first period. However, differing from the H-H clustering, most of the L-L clustering was strong extra cooling service accessibility, while the moderate extra cooling service accessibility was minor.

Overall, the abnormal clustering patterns were fewer, and most of the grids were H-L, L-H, not significant clustering, which demonstrates the general recognition that residents with higher cooling service accessibility tends to face lower heat exposure risk. Albeit the improvement of UGS and decrease in HIA in 2020 compared to in 2010, the spatial clustering revealed that the residents-perceived thermal environment may have deteriorated when considering the spatial interaction effect among residents, UGS and HIA. In other words, more and more residents were aggregated in locations where they could suffer from extra heat exposure while fewer and fewer residents were located where they could access extra cooling service.

4. Discussion

4.1. Interaction between UGS and HIA

Generally, rapid urbanization process is known to encroach upon green space, leading to its fragmentation and shrinkage. This results in deterioration of urban thermal environment. This interaction among urbanization, UGS and UHI effect is evident in many developing cities worldwide. For example, Chinese cities of Fuzhou and Dalian (Yang et al., 2017; Yu et al., 2018); Indian city of Raiganj (Basu and Das, 2023); Brazilian city of Paço do Lumiar (Silva et al., 2018). However, in the case of the city of Zhengzhou, the trend was found to be the opposite due to the implementation of forest city project. This project has led to a significant improvement of UGS, especially within the inner city. A corresponding decrease in the HIA was observed in 2020 as compared to 2010.

As a rapidly developing city, Zhengzhou is a paradigm that has attracted many scholars. Consistent findings were reported by researchers such as Yang et al. (2022), where they indicated an increase in the city's UGS and mitigation of the UHI effect. The effort of forest project also was recognized in their study.

In fact, the improvement in UGS, especially for the area, is expected to significantly enhance the urban thermal environment (Li et al., 2020; Tan et al., 2021). Nonetheless, the cooling effect also could be influenced by many landscape characteristics besides the area (Xiao et al., 2023). As suggested by Xiao et al. (2018), the green space may have no cooling effect and even has higher temperature if its area is small. Manoli et al. (2019) also proved that besides UGS, the magnitude of UHI effect could be largely explained by population and climate. The two considerations on some occasions are even more preponderant than UGS. Apparently, there would be marginal difference in climate in city-level study and the newly added UGS may have worse cooling pattern and smaller area due to the fixed development level in the city core.

Accordingly, the increase of HIA in 2020 within the 3rd ring road could be mostly ascribed to the population agglomeration and UGS cooling landscape pattern. Despite this, the thermal environment was found to have generally improved in 2020 compared to 2010.

4.2. Accessibility-based cooling service and heat exposure risk

In this study, the spatial pattern of cooling service accessibility, decreasing from the inside to the outside, is consistent with Lan et al. (2022), but contrary to M. Chen et al. (2022) who indicated that most of residents in suburbs may not be able to access sufficient cooling service while the residents in the city center could better access cooling service. The opposite finding could be ascribed to the different quantification scope of UGS. M. Chen et al. (2022) only accounted the cooling service by urban parks, neglecting the role of non-park UGS, which is important in cooling service equity (Ke et al., 2023).

Notably, there was a dramatic increase of cooling service accessibility in the northwest and southeast periphery in 2020. It is likely due to the implementation of several large greenery projects, such as Diehu Forest Park, Chaohu Wetland, and Yellow River Cultural Park in recent years. However, the overall accessibility level in the periphery (beyond the 4th ring road) even decreased, and the inequity further enlarged. In contrast, the increase in UGS within the 3rd road not only improved the overall accessibility level but also narrowed the inequity (Fig. 5).

The inequity festered by large greening projects outside the 4th ring road is also corroborated by heat exposure risk. In this zone, growing areas were inaccessible to HIA over the time, while the overall heat exposure risk level also increased. This is mainly because the large green parks were implemented in the outskirt, and thus the HIA surrounding these parks has largely shrunk, saliently reducing the possibility of contiguous residents exposed to heat risk. However, a few residents not close to these greening parks may suffer from deteriorated thermal environment.

Our results on accessibility-based heat exposure risk differ from Li et al. (2023) who identified that residents in Shenzhen downtown are less heat risk than in the outskirt. The difference is because they appeared to believe that more people aggregated around the heat risk areas would instead mitigate the severity of the heat risk and used division, similar to a supply/demand ratio like UGS accessibility, to deal with the relationship between population and heat risk areas.

4.3. Abnormal clustering pattern and spatial interaction effect

The H-H clustering, meaning that residents still are exposed to higher heat risk with affluent available cooling service, is a disadvantageous clustering pattern that should be focused on. In Chinese cities, the manufacturing industries tend to gather around suburban areas due to cost and pollution concerns (Wang et al., 2020; Wu et al., 2018). In Zhengzhou, a large number of secondary industries are clustered around the 4th ring road, which is the demarcation of suburban areas and the outer suburbs. The 4th ring road is also a primary road with intensive traffic flow. This locational feature will inevitably lead to extra anthropogenic pollution emissions, including heat emissions, causing surrounding residents being exposed to extra heat risk despite the availability of adequate cooling services (Koralegedara et al., 2016; Murray and Heggie, 2016).

Over the past decade, Zhengzhou attracted a large number of inhabitants because of the rapid economic development of the city. Accordingly, there has been a massive outward expansion of residential areas in order to encounter increasingly thronged population, with some residential quarters even being built around industrial areas (Wang et al., 2022). Therefore, despite the decrease in HIA with the improvement of UGS, an increasing number of people are residing around disadvantageous quarters where they have to face extra heat exposure risk if spatial interaction effect is considered.

Furthermore, the urban sprawl has infringed upon natural green spaces and water bodies. Due to different landscape characteristics with artificial green infrastructure, these natural green spaces may purvey greater cooling effect than small and decentralized UGS created by the forest project (Gunawardena et al., 2017; Zhou et al., 2023), resulting in the advantageous locations where residents could receive extra cooling effect largely shrunk.

4.4. Accessibility-based assessment: improvement and practicality

This study proposes a novel urban thermal environment assessment framework in terms of accessibility. It considers population as the demand point, and UGS and HIA as the supply points. Unlike traditional studies that rely on the linear integration of associated indicators (Chen et al., 2021; Tieskens et al., 2022; Shen et al., 2022; Li et al., 2022a; Zhu and Yuan, 2023), this study employs an improved 2SFCA method. This method allows for the incorporation of the spatial interaction effects among residents, UGS, and HIA. By considering the effect, we are able to measure the residents-perceived thermal environment on the basis of spatiotemporal changes of UGS and HIA. Furthermore, as the thermal environment is quantified in two opposite aspects, namely cooling service accessibility and heat exposure risk, this study could assess the rationality of residents' aggregation pattern and identify the locations that are disadvantageous and advantageous for resident congregation by spatial autocorrelation analysis, except for the accessibility-based cooling service and heat exposure risk assessment. However, these abnormal clustering patterns are seldom involved in traditional thermal comfort evaluation studies.

In addition, this study mainly depends on Landsat imageries and WorldPop data, making it a simple and replicable method, and it could thus be easily applied in other cities all over the world.

4.5. Planning and policy implications

The spatial autocorrelation analysis reveals a growing number of residents are aggregating in disadvantageous locations, warranting special attention. The first priority is to minimize the spatial interaction between residents and HIA. On one hand, we propose establishing a clear division of industrial areas and preventing the sprawl of industrial zones into residential communities. Additionally, the upgrading of industries, with a priority to reduce secondary industries with high emissions near densely highly populated areas, should also be accelerated. On other hand, urban planning should also aim to limit the new residential development around industrial zones and primary traffic roads to reduce residents' aggregation as well as exposure to extra heat risk. The use of cleaner fuels, changing transportation mode from car to bus and the development of electric vehicles also could be promoted to decrease urban anthropogenic heat emissions around the primary traffic roads (Ribeiro et al., 2021).

In the highly developed city center, the land price is much more exorbitant than in the outskirt, making increasingly enhancing UGS coverage inadvisable. We suggest paying close attention to optimizing the quality (NDVI) and landscape patterns of UGS in response to population growth. However, the impact of landscape pattern on cooling effect remains controversial. For example, Zhou et al. (2022) corroborated that the UGS with an irregular shape can produce a more substantial cooling effect while an opposite result was found by Liao et al. (2023). Thus, focusing on the improvement in quality of UGS is presumably a more univocal management. Moreover, the small and evenly-decentralized green infrastructure with minimal cooling threshold could be easily woven into the residential communities so that it could better improve the residents' cooling service accessibility than large greening project under given areas (Yan et al., 2021).

4.6. Limitations and future directions

First, the WorldPop data, applied as the demand point in the accessibility quantification, is a quiescent population spatial distribution data with a temporal resolution of one year. However, considering the high mobility of urban dwellers, their access to cooling service and faced heat exposure risk may thereby vary. Subsequent studies should consider adopting dynamic population data, potentially utilizing resources such as Baidu heatmaps or social media check-in data. Second, the Gaussian function was used to describe the decay effect of cooling service and heat risk over distance. To provide a more accurate account of this decay effect, it is recommended that future research adopts advanced mathematical functions, or employs regression analyses, to more robustly quantify the cooling effect and heat risk prior to the accessibility-based evaluation. Moreover, it is proposed to optimize the quality index by incorporating more indicators associated with the cooling effect and heat risk to reduce the uncertainty from single indicators.

5. Conclusions

Compared to traditional assessments, which usually depended on linear integration of associated indicators, this study used the improved 2SFCA method to consider the spatial interaction effect among residents, UGS, and HIA. By incorporating the effect, we were able to examine the rationality of residents' aggregation pattern in Zhengzhou and identify the locations that are disadvantageous and advantageous for resident congregation. The results revealed an improvement of UGS and decrease of HIA in 2020 compared to 2010. However, when considering the spatial interaction effect, residents' heat exposure risk actually increased despite the reduction in HIA. Especially in the periphery, the inequality of cooling service accessibility and heat exposure risk further increased. Spatial clustering pattern suggested that an increasing number of residents were gathering in disadvantageous locations where they could suffer from extra heat risk exposure, while fewer and fewer residents were located in advantageous areas available to extra cooling service.

Based on the findings, we propose optimizing the landscape pattern of UGS within inner city, and establishing a clear division of industrial areas in order to prevent the sprawl of industrial land into residential zones. Urban planning should also aim to limit residential development near industrial zones and primary traffic roads to minimize residents' exposure to extra heat risk. The developed method provides a viable accessibility-based assessment for the urban thermal environment with a finer resolution, which could serve as a guide for the improvement of the urban thermal environment, especially assisting urban planners in targeting these disadvantageous locations where residents could suffer from extra heat exposure risk.

Declaration of competing interests

The authors declare that they have no known competing financial interests or personal relationships that could have appeared to influence the work reported in this paper.

Acknowledgements

This work was funded by the Major Project of the National Social Science Foundation of China (Grant No. 19ZDA088) and the National Natural Science Foundation of China Projects (Grant No. 72204101).

References

Basu, T., Das, A., 2023. Urbanization induced degradation of urban green space and its association to the land surface temperature in a medium-class city in India. Sustain. Cities Soc. 90, 104373.

Battista, G., de Lieto Vollaro, E., Ocłoń, P., de Lieto Vollaro, R., 2023. Effects of urban heat island mitigation strategies in an urban square: a numerical modelling and experimental investigation. Energe Build. 282, 112809.

Chen, B., Xie, M., Feng, Q., Li, Z., Chu, L., Liu, Q., 2021. Heat risk of residents in different types of communities from urban heat-exposed areas. Sci. Total Environ. 768, 145052.

Chen, B., Xie, M., Feng, Q., Wu, R., Jiang, L., 2022. Diurnal heat exposure risk mapping and related governance zoning: a case study of Beijing, China. Sustain. Cities Soc. 81, 103831.

Chen, M., Jia, W., Yan, L., Du, C., Wang, K., 2022. Quantification and mapping cooling effect and its accessibility of urban parks in an extreme heat event in a megacity. J. Clean. Prod. 334, 130252.

Conti, S., Meli, P., Minelli, G., Solimini, R., Toccaceli, V., Vichi, M., 2005. Epidemiologic study of mortality during the Summer 2003 heat wave in Italy. Environ. Res. 98, 390–399.

Das, M., Das, A., Momin, S., 2022. Quantifying the cooling effect of urban green space: a case from urban parks in a tropical mega metropolitan area (India). Sustain. Cities Soc. 87, 104062.

Dutta, I., Das, A., 2020. Exploring the spatio-temporal pattern of regional heat island (RHI) in an urban agglomeration of secondary cities in Eastern India. Urban Clim. 34, 100679.

Feng, Y., Gao, C., Tong, X., Chen, S., Lei, Z., Wang, J., 2019. Spatial patterns of land surface temperature and their influencing factors: a case study in Suzhou, China. Remote Sens. 11 (2), 182.

Foley, J.A., DeFries, R., Asner, G.P., Barford, C., Bonan, G., Carpenter, S.R., 2005. Global consequences of land use. Science 309, 570–574.

Gunawardena, K.R., Wells, M.J., Kershaw, T., 2017. Utilising green and bluespace to mitigate urban heat island intensity. Sci. Total Environ. 584-585, 1040–1055.

Halder, B., Bandyopadhyay, J., Banik, P., 2021. Monitoring the effect of urban development on urban heat island based on remote sensing and geo-spatial approach in Kolkata and adjacent areas, India. Sustain. Cities Soc. 74, 103186.

Ke, X., Huang, D., Zhou, T., Men, H., 2023. Contribution of non-park green space to the equity of urban green space accessibility. Ecol. Indic. 146, 109855.

Koralegedara, S.B., Lin, C.Y., Sheng, Y.F., Kuo, C.H., 2016. Estimation of anthropogenic heat emissions in urban Taiwan and their spatial patterns. Environ. Pollut. 215, 84–95.

Chmura Kraemer, H., Periyakoil, V.S., Noda, A., 2002. Kappa coefficients in medical research. Stat. Med. 21, 2109–2129.

Lan, T., Liu, Y., Huang, G., Corcoran, J., Peng, J., 2022. Urban green space and cooling services: opposing changes of integrated accessibility and social equity along with urbanization. Sustain. Cities Soc. 84, 104005.

Lee, W., Choi, H.M., Lee, J.Y., Kim, D.H., Honda, Y., Kim, H., 2018. Temporal changes in mortality impacts of heat wave and cold spell in Korea and Japan. Environ. Int. 116, 136–146.

Li, L., Zha, Y., Zhang, J., 2020. Spatially non-stationary effect of underlying driving factors on surface urban heat islands in global major cities. Int. J. Appl. Earth Obs. Geoinf. 90, 102131.

Li, H., Zhou, W., Wang, W., Zheng, Z., 2022a. Imbalanced supply and demand of temperature regulation service provided by urban forests: a case study in Shenzhen, China. Ecol. Indic. 145, 109666.

Li, J., Fang, Z., Zhang, J., Huang, Q., He, C., 2022b. Mapping basin-scale supply-demand dynamics of flood regulation service – a case study in the Baiyangdian Lake Basin, China. Ecol. Indic. 139, 108902. doi:10.1016/j.ecolind.2022.108902.

Li, B., Zhang, B., Yin, L., Chang, J., 2023. Assessing heat risk for residents of complex urban areas from an accessibility-based perspective. Sustain. Cities Soc. 88, 104278.

Liao, W., Guldmann, J.M., Hu, L., Cao, Q., Gan, D., Li, X., 2023. Linking urban park cool island effects to the landscape patterns inside and outside the park: a simultaneous equation modeling approach. Landsc. Urban Plan. 232, 104681.

Liu, Z., Zhan, W., Bechtel, B., Voogt, J., Lai, J., Chakraborty, T., 2022. Surface warming in global cities is substantially more rapid than in rural background areas. Commun. Earth Environ. 3, 219.

Luo, W., Wang, F., 2003. Measures of spatial accessibility to health care in a GIS environment: synthesis and a case study in the Chicago region. Environ. Plan. B: Plan. Des. 30, 865–884.

Manoli, G., Fatichi, S., Schläpfer, M., Yu, K., Crowther, T.W., Meili, N., 2019. Magnitude of urban heat islands largely explained by climate and population. Nature 573, 55–60.

Martilli, A., Krayenhoff, E.S., Nazarian, N., 2020. Is the urban heat island intensity relevant for heat mitigation studies? Urban Clim. 31, 100541.

Murray, J., Heggie, D., 2016. From urban to national heat island: the effect of anthropogenic heat output on climate change in high population industrial countries. Earths Future 4, 298–304.

Newbold, T., Hudson, L.N., Hill, S.L.L., Contu, S., Lysenko, I., Senior, R.A., 2015. Global effects of land use on local terrestrial biodiversity. Nature 520, 45–50.

Nimac, I., Herceg-Bulić, I., Žuvela-Aloise, M., 2022. The contribution of urbanisation and climate conditions to increased urban heat load in Zagreb (Croatia) since the 1960s. Urban Clim. 46, 101343.

Park, C.Y., Thorne, J.H., Hashimoto, S., Lee, D.K., Takahashi, K., 2021a. Differing spatial patterns of the urban heat exposure of elderly populations in two megacities identifies alternate adaptation strategies. Sci. Total Environ. 781, 146455.

Park, C.Y., Park, Y.S., Kim, H.G., Yun, S.H., Kim, C.K., 2021b. Quantifying and mapping cooling services of multiple ecosystems. Sustain. Cities Soc. 73, 103123.

Patz, J.A., Campbell-Lendrum, D., Holloway, T., Foley, J.A., 2005. Impact of regional climate change on human health. Nature 438, 310–317.

Radke, J., Mu, L., 2000. Spatial decompositions, modeling and mapping service regions to predict access to social programs. Geogr. Inf. Sci. 6, 105–112.

Rajagopal, P., Priya, R.S., Senthil, R., 2023. A review of recent developments in the impact of environmental measures on urban heat island. Sustain. Cities Soc. 88, 104279.

Ribeiro, F.N.D., Umezaki, A.S., Chiquetto, J.B., Santos, I., Machado, P.G., Miranda, R.M., 2021. Impact of different transportation planning scenarios on air pollutants, greenhouse gases and heat emission abatement. Sci. Total Environ. 781, 146708.

Scortichini, M., de'Donato, F., De Sario, M., Leone, M., Åström, C., Ballester, F., 2018. The

inter-annual variability of heat-related mortality in nine European cities (1990–2010). Environ. Health. 17, 66.
Sekertekin, A., 2019. Validation of physical radiative transfer equation-based land surface temperature using Landsat 8 satellite imagery and SURFRAD in-situ measurements. J. Atmos. Sol.-Terr. Phys. 196, 105161.
Shen, Z.J., Zhang, B.H., Xin, R.H., Liu, J.Y., 2022. Examining supply and demand of cooling effect of blue and green spaces in mitigating urban heat island effects: a case study of the Fujian Delta urban agglomeration (FDUA), China. Ecol. Indic. 142, 109187.
Silva, J.S., Silva, R.M.D., Santos, C.A.G., 2018. Spatiotemporal impact of land use/land cover changes on urban heat islands: a case study of Paço do Lumiar, Brazil. Build. Environ. 136, 279–292.
Smith, I.A., Fabian, M.P., Hutyra, L.R., 2023. Urban green space and albedo impacts on surface temperature across seven United States cities. Sci. Total Environ. 857, 159663.
Tan, J., Zheng, Y., Tang, X., Guo, C., Li, L., Song, G., 2010. The urban heat island and its impact on heat waves and human health in Shanghai. Int. J. Biometeorol. 54, 75–84.
Tan, X., Sun, X., Huang, C., Yuan, Y., Hou, D., 2021. Comparison of cooling effect between green space and water body. Sustain. Cities Soc. 67, 102711.
Tieskens, K.F., Smith, I.A., Jimenez, R.B., Hutyra, L.R., Fabian, M.P., 2022. Mapping the gaps between cooling benefits of urban greenspace and population heat vulnerability. Sci. Total Environ. 845, 157283.
UN DESA, 2018. World Urbanization Prospects: The 2018 Revision. United Nations Department of Economic and Social Affairs.
Wang, K., Li, G., Liu, H., 2020. Location choice of industrial land reduction in Metropolitan Area: evidence from Shanghai in China. Growth Change 51 (4), 1837–1859.
Wang, Y., Chang, Q., Fan, P., 2021. A framework to integrate multifunctionality analyses into green infrastructure planning. Landsc. Ecol. 36, 1951–1969.
Wang, S., Guo, W., Shen, L., Huang, J., 2022. Spatial and temporal differences of urban land expansion pattern and utilization intensity in Zhengzhou City. Prog. Geogr. 41, 385–395.
Wong, L.P., Alias, H., Aghamohammadi, N., Aghazadeh, S., Nik Sulaiman, N.M., 2017. Urban heat island experience, control measures and health impact: a survey among working community in the city of Kuala Lumpur. Sustain. Cities Soc. 35, 660–668.
Wu, J., Wei, Y.D., Li, Q., Yuan, F., 2018. Economic transition and changing location of manufacturing industry in China: a study of the Yangtze River Delta. Sustainability 10 (8), 2624.
Xi, C., Wang, D., Cao, S.J., 2023. Impacts of trees-grass area ratio on thermal environment, energy saving, and carbon benefits. Urban Clim. 47, 101393.
Xiao, X.D., Dong, L., Yan, H., Yang, N., Xiong, Y., 2018. The influence of the spatial characteristics of urban green space on the urban heat island effect in Suzhou Industrial Park. Sustain. Cities Soc. 40, 428–439.
Xiao, Y., Piao, Y., Pan, C., Lee, D., Zhao, B., 2023. Using buffer analysis to determine urban park cooling intensity: five estimation methods for Nanjing, China. Sci. Total Environ. 868, 161463.
Xing, L., Liu, Y., Wang, B., Wang, Y., Liu, H., 2020. An environmental justice study on spatial access to parks for youth by using an improved 2SFCA method in Wuhan, China. Cities 96, 102405.
Yan, H., Wu, F., Dong, L., 2018. Influence of a large urban park on the local urban thermal environment. Sci. Total Environ. 622-623, 882–891.
Yan, L., Jia, W., Zhao, S., 2021. The cooling effect of urban green spaces in metacities: a case study of Beijing, China's Capital. Remote Sens. 13, 2021.
Yang, J., Sun, J., Ge, Q., Li, X., 2017. Assessing the impacts of urbanization-associated green space on urban land surface temperature: a case study of Dalian, China. Urban For. Urban Green. 22, 1–10.
Yang, Y., Song, F., Ma, J., Wei, Z., Song, L., Cao, W., 2022. Spatial and temporal variation of heat islands in the main urban area of Zhengzhou under the two-way influence of urbanization and urban forestry. PLoS One 17 (8), e0272626.
Yang, J., Duan, C., Wang, H., Chen, B., 2023. Spatial supply-demand balance of green space in the context of urban waterlogging hazards and population agglomeration. Resour. Conserv. Recycl. 188, 106662.
Yao, L., Liu, J., Wang, R., Yin, K., Han, B., 2014. Effective green equivalent—a measure of public green spaces for cities. Ecol. Indic. 47, 123–127.
Yao, X., Yu, K., Zeng, X., Lin, Y., Ye, B., Shen, X., 2022. How can urban parks be planned to mitigate urban heat island effect in "Furnace cities" ? An accumulation perspective. J. Clean. Prod. 330, 139582.
Yu, X., Guo, X., Wu, Z., 2014. Land surface temperature retrieval from Landsat 8 TIRS—comparison between radiative transfer equation-based method, split window algorithm and single channel method. Remote Sens. 6, 2014.
Yu, Z., Guo, X., Zeng, Y., Koga, M., Vejre, H., 2018. Variations in land surface temperature and cooling efficiency of green space in rapid urbanization: the case of Fuzhou city, China. Urban For. Urban Green. 29, 113–121.
Zhang, W., Jiang, J.G., Zhu, Y.B., 2015. Spatial-temporal evolution of urban thermal environment based on spatial statistical features. Chin. J. Appl. Ecol. 26, 1840–1846 (in Chinese).
Zhang, J., Zhang, D., Huang, L., Wen, H., Zhao, G., Zhan, D., 2019. Spatial distribution and influential factors of industrial land productivity in China's rapid urbanization. J. Clean. Prod. 234, 1287–1295.
Zhang, G., Zeng, G., Liang, X.Z., Huang, C., 2021. Increasing heat risk in China's urban agglomerations. Environ. Res. Lett. 16, 064073.
Zhang, R., Peng, S., Sun, F., Deng, L., Che, Y., 2022. Assessing the social equity of urban parks: an improved index integrating multiple quality dimensions and service accessibility. Cities 129, 103839.
Zhou, D., Zhao, S., Zhang, L., Sun, G., Liu, Y., 2015. The footprint of urban heat island effect in China. Sci. Rep. 5, 11160.
Zhou, W., Yu, W., Wu, T., 2022. An alternative method of developing landscape strategies for urban cooling: a threshold-based perspective. Landsc. Urban Plan. 225, 104449.
Zhou, W., Cao, W., Wu, T., Zhang, T., 2023. The win-win interaction between integrated blue and green space on urban cooling. Sci. Total Environ. 863, 160712.
Zhu, W., Yuan, C., 2023. Urban heat health risk assessment in Singapore to support resilient urban design — by integrating urban heat and the distribution of the elderly population. Cities 132, 104103.